Designing Slow-Light Photonic Crystal Waveguides for Four-Wave Mixing Applications

Panagiotis Kanakis,[1*] Thomas Kamalakis,[2] Thomas Sphicopoulos,[1]

[1]*Department of Informatics and Telecommunications, National and Kapodistrian University/Athens, Panepistimioupolis, Athens GR157 84, Greece*
[2]*Department of Informatics and Telematics, Harokopio University/Athens, 9 Omirou Street, Athens GR17778, Greece*
*Corresponding author: kanakis@di.uoa.gr

We discuss the optimization of photonic crystal waveguides for four-wave mixing applications, taking into account linear loss and free-carrier effects. Suitable figures-of-merits are introduced in order to guide us through the choice of practical, high efficiency designs requiring relatively low pump power and small waveguide length. In order to realistically perform the waveguide optimization process, we propose and validate an approximate expression for the four-wave mixing efficiency, which significantly alleviates our numerical calculations. Promising waveguide designs are identified by means of exhaustive search, altering some structural parameters. Our approach aims at optimizing the waveguides for nonlinear signal-processing applications based on the four-wave mixing.
OCIS Codes: (190.4380) Nonlinear optics, four-wave mixing, (130.5296) Photonic crystal waveguides.

Four-wave mixing (FWM) bears great promise for achieving signal processing functionalities in future optical networks such as wavelength conversion, signal regeneration/reshaping, time division demultiplexing, etc [1-3]. Degenerate FWM consists of the nonlinear interaction between three co-propagating waves (pump, signal and idler). The most commonly used figure-of-merit (FoM) for evaluating FWM is the conversion efficiency η defined as:

$$\eta \equiv P_i(L)/P_s(0) \tag{1}$$

where $P_i(L)$ is the power of the idler wave at the output of the waveguide (of length L), and $P_s(0)$ is the incident power of the signal wave. The efficiency depends not only on the waveguide parameters but on the choice of signal and idler wavelengths λ_s and λ_i respectively as well as the incident pump power P_0. The quest for a waveguide design that exhibits large values of η, is the most common task undertaken by many authors. Coupled resonators optical waveguides (CROW), highly nonlinear fibers (HNLF), and photonic crystal waveguides (PCWs), are examples of photonic structures that are currently attracting attention in that respect [4-7].

Simply achieving a large η is not always sufficient in many applications, since other important aspects need to be evaluated. For a given length L and pump power P_0, one should also be interested in the available bandwidth, which can be quantified in terms of the optical pump wavelength range $\Delta\lambda$ in which η does not fall below a certain level (say -3dB) of its maximum value $\eta_0(P_0,L)$. Tunability is also another important aspect and can be quantified as the wavelength separation $\delta\lambda$ between the pump and the signal waves for which η is again higher than -3dB compared to η_0. These parameters are more thoroughly explained further below. We are therefore led to a more suitable FoM, defined by the product of the maximum efficiency, the bandwidth and the tunability (EBT):

$$\text{EBT} = \max_{\{P_0, L\}} \{\eta_0 \times \Delta\lambda \times \delta\lambda\} \tag{2}$$

where the maximum is taken over an appropriate wide range of values for P_0 and L. A large EBT value should ensure a smooth wavelength dependence for η which is important in wavelength division multiplexing systems. Also, since modern trends in optical research dictate the use of compact, low-power components we may also use a more power and size aware FoM,

$$\text{EBT}_{\text{PL}} = \max_{\{P_0, L\}} \left\{ \frac{\eta_0 \times \Delta\lambda \times \delta\lambda}{P_0 \times L} \right\} \tag{3}$$

For an individual waveguide design, we estimate $\eta(\lambda_i, \lambda_s, P_0, L)$ on a multi-grid of $(\lambda_i, \lambda_s, P_0, L)$ values. For each pair of (P_0, L) we estimate η_0, $\delta\lambda$ and $\Delta\lambda$, numerically as explained below, and use Eqs. (2) and (3) to obtain the EBT or EBT$_{\text{PL}}$ values. Various waveguide designs can therefore be compared on the basis of their EBT or EBT$_{\text{PL}}$ values. To estimate the proposed FoMs for a given design, it is evident that $\eta(\lambda_i, \lambda_s, P_0, L)$ must be computed in a four parameter space $(\lambda_i, \lambda_s, P_0, L)$ and if one compares many different designs the required number of computations grows significantly. An efficient calculation of η is therefore of vital importance.

In this work, we apply this design optimization method in the case of PCWs by means of exhaustive search after discussing an efficient way of obtaining η. PCWs combine large slowdown factors and sub-wavelength light
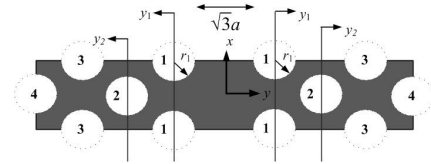

Figure1. A PCW formed by embedding air holes in a thin layer of silicon. The numbers indicate the hole class according to their proximity to the waveguide defect while arrows indicate the structural perturbation.

confinement leading to an enhancement of nonlinear effects like FWM. A photonic crystal slab is formed by embedding a two-dimensional array of holes of low refractive index material (e.g. air) inside a thin film of higher index material (e.g. silicon). Removing an entire row of holes, as illustrated in Figure 1, introduces a defect mode thereby effectively forming a PCW. The remaining holes can be classified according to their proximity to the waveguide defect, i.e. the 1st class is located closest to the defect and so forth, as shown in Figure 1. Altering a few structural characteristics, it is possible to minimize the group velocity dispersion, creating a nearly linear region in the dispersion relation which corresponds to a flat wavelength dependence of the group index n_g [7]. This wavelength region is usually referred to as the flat-band region. The PCW dispersion relation and the guided mode fields are obtained by a 3D plane-wave expansion mode solver implemented in MATLAB [8]. The dispersion characteristics (e.g. n_g) are calculated through polynomial fitting on dispersion relation of the guided mode [8].

The FWM conversion efficiency can be calculated by numerically solving the coupled ordinary differential equations (ODEs) for the three propagating waves recently derived in the case of PCWs [9]. Given the multi-parameter space, that needs to be considered in the estimation of EBT and EBT$_{PL}$, we have found that numerical solution of the ODEs generally leads to impractical computational times. We instead estimate η with a much faster, approximate expression. To obtain this expression, we generalize a technique previously applied when only linear losses are present [10]: We use the lossless FWM efficiency formula and account for the pump power variation across the waveguide by replacing the incident pump power P_0 with the average pump power $\overline{P_p} = \frac{1}{L}\int_0^L P_p(z)dz$ in order to account for the power loss induced in the pump wave. We also account for the linear loss experienced by the idler wave [10]. To accurately estimate the pump power variation $P_p(z)$ in silicon we need to include the nonlinear two-photon absorption (TPA) and the free-carrier (FC) effects [9]. However, the latter loss contribution is significantly more important. Thus, by neglecting TPA nonlinear losses, the evolution of the pump power will be determined by [11]:

$$dP_p / dz \cong -\left(a_p + 2F_p P_p^2\right)P_p \qquad (4)$$

where a_p is linear loss coefficient for the pump wave and F_p is the free-carrier effect coefficient determined by [9]:

$$F_\mu \cong \frac{N_C}{P_p^2}\left(j\frac{2\pi}{\lambda_\mu}C_1 - \frac{C_2}{2}\right)\left(\frac{\lambda_\mu}{\lambda_0}\right)^2 \qquad (5)$$

In Eq. (5), $\mu=p,s$ or i (corresponding to pump, signal and idler waves, respectively), $N_C=\beta_{TPA}S_p^3\tau_C P_p^2/(2\hbar\omega_p A_{ppp}^2)$ is the free-carrier density [9,12], λ_μ is the corresponding wavelength, $\lambda_0=1550$nm, β_{TPA} is the TPA coefficient, S_μ is the slow-down factor and τ_C is the free-carrier life-time.
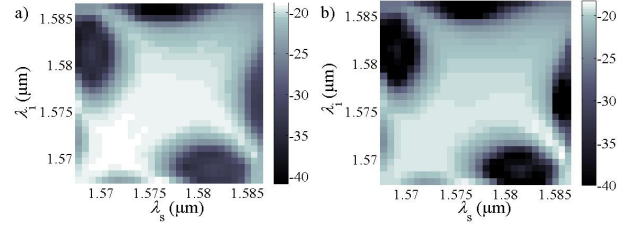

Figure 2. FWM conversion efficiency with respect to the wavelength of the idler (λ_i) and the signal (λ_s) waves obtained (a) numerically solving the ODEs and (b) using (11).

The effective modal areas are determined by the modal fields as [9]:

$$A_{\rho\kappa\psi} = \frac{\int_V |E_\rho|^2\,dV\left(\int_V |E_\kappa|^2\,dV\int_V |E_\psi|^2\,dV\right)^{1/2}}{a\int_V E_\rho^* E_\rho^* E_\kappa E_\psi\,dV} \qquad (6)$$

using numerical integration. In Eq. (6), V is the volume of the waveguide supercell, E_μ is the electric field component for wave μ along the y-direction and a is the lattice constant of the waveguide. The selection of only the transverse y-component is made based on the fact that for TE-like guided modes the component along the x-direction contains only a small fraction of the wave power. For silicon waveguides, we use the values $C_1=1.35\times10^{-27}$m^3 and $C_2=1.45\times10^{-21}$m^2 [9]. Equation (4), can be solved analytically to yield:

$$P_p(z) = P_0 e^{-a_p z}\left(1+\delta(1-e^{-2a_p z})\right)^{-1/2} \qquad (7)$$

where $\delta=2a_p^{-1}\text{Re}\{F_p\}P_p(0)^2$, while using standard integration formulas, we obtain the following expressions:

$$\overline{P_P} = -\frac{P_0}{a_p L\sqrt{\delta}}\left\{\sin^{-1}\left(\frac{e^{-a_p L}}{\sqrt{\delta^{-1}+1}}\right) - \sin^{-1}\left(\frac{1}{\sqrt{\delta^{-1}+1}}\right)\right\} \qquad (8)$$

$$\overline{P_p^2} = \frac{1}{L}\int_0^L P_p^2(z)dz = \frac{P_0^2}{2a_p\delta}\ln\left(1+\delta\left(1-e^{-2a_p L}\right)\right) \qquad (9)$$

The losses experienced by the idler wave are given by:

$$l_i = P_i(L)/P_i(0) = \exp\left(-a_i L + 2L\,\text{Re}\{F_i\}\overline{P_p^2}\right) \qquad (10)$$

where a_i is the linear loss coefficient of the idler wave. Extending the method in [10], the efficiency is written as:

$$\eta = l_i\frac{\lambda_s}{\lambda_i}\left(1+\frac{\kappa_{tot}^2}{4g^2}\right)\sinh^2(gL) \qquad (11)$$

In Eq. (11), $\kappa_{tot} = \kappa + \text{Im}\left\{F_s + F_i - 2F_p\right\}\overline{P_p^2}$ is the total phase mismatch while κ is the phase mismatch in the presence of linear losses only and g is the parametric gain, given by:
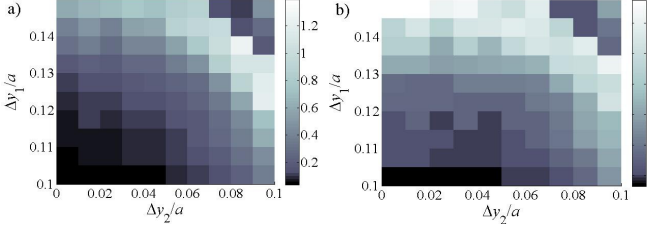
Figure 3. (a) EBT and (b) EBT$_{PL}$ values with respect to the design parameters Δy_1 and Δy_2.

$$\kappa = \Delta k + 4\pi n_2 \overline{P}_p \left(A_{pss}^{-1}\lambda_s^{-1} + A_{pii}^{-1}\lambda_i^{-1} - A_{ppp}^{-1}\lambda_p^{-1} \right) \qquad (12)$$

$$g = \left(n_2^2 S_p^2 S_i S_s \omega_i \omega_s \overline{P}_p c^{-2} A_{psi}^{-2} - \kappa^2 / 4 \right)^{1/2} \qquad (13)$$

where $\omega_\mu = 2\pi c/\lambda_\mu$, Δk is the linear phase mismatch [10], c is the speed of light in vacuum and n_2 is the nonlinear Kerr coefficient. The linear loss coefficients a_μ are calculated using the loss model proposed in [7],[8]. In our work, a silicon PCW slab embedded in air is assumed. To validate the analytical formulas, we plot in Figure 2, the values of η in the case of a PCW obtained by perturbing the positions of all first class holes by $\Delta y_1 = 0.148a$ for $P_0 = 0.4W$ and $L = 400\mu m$. In our calculations throughout the paper, we assume that $P_s(0) = 0.5mW$, $\tau_C = 600ps$, $\beta_{TPA} = 5\times10^{-11}m/W$ while the slab height is $h = 0.5a$ and the lattice constant is $a = 412nm$. Unless specified otherwise, the radii of all holes are equal to $r = 0.27a$. In Figure 2, the values of η with respect to all possible wavelength combinations (λ_s,λ_i), inside the flat-band region are shown. The flat-band region is defined as the wavelength range in which n_g varies no more than $\pm 10\%$ from the n_g value at the point where the group velocity dispersion coefficient is minimum. The wavelength distance between the idler and signal waves, $|\lambda_i - \lambda_s|$, is always taken larger than 0.1nm. Figure 2(a) presents the values obtained by solving the ODEs using a Runge Kutta scheme [13], when a quasi-continuous wave regime is assumed taking into account the TPA nonlinear loss term ignored in Eq. (11), while Figure 2(b) plots the values obtained by Eq. (11). The figure shows that the two methods are in very good agreement despite the fact that the TPA nonlinear losses in Eq. (11) are neglected. We estimated the average error to be approximately 0.5dB for the wavelength combinations where the ODE efficiency is not smaller than -10dB from its maximum value, $\eta_0 \cong -19dB$. We have observed that using the analytical formula yields a significant speedup in computational time of at least one order of magnitude.

Once $\eta(\lambda_s,\lambda_i)$ is obtained, we proceed to calculate $\Delta\lambda$ and $\delta\lambda$ for given values of P_0 and L. For every pair (λ_s,λ_i) for which the efficiency $\eta(\lambda_s,\lambda_i) \geq \eta_0/2$ ($\geq$-3dB), we estimate the corresponding pump wavelength λ_p and the wavelength detuning $|\lambda_p - \lambda_s|$. The range of values of λ_p determines the bandwidth $\Delta\lambda(P_0,L) \equiv \max(\lambda_p) - \min(\lambda_p)$ ($\cong$18nm for the case of Figure 2). To calculate $\delta\lambda(P_0,L)$ we take the average of the detuning values $|\lambda_p - \lambda_s|$ ($\cong$3nm for Figure 2). Note that $\delta\lambda$ is calculated as the average rather than the range of detuning values. This is because, referring to Figure 2, one can see that for some combinations of (λ_i,λ_s), high
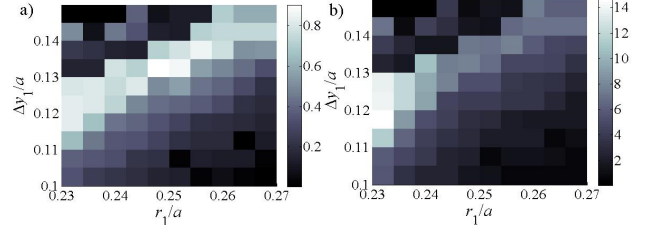

Figure 4. (a) EBT and (b) EBT$_{PL}$ values with respect to the design parameters Δy_1 and r_1.

efficiencies are obtained even at large $|\lambda_i - \lambda_s|$ or equivalently $|\lambda_p - \lambda_s|$ (e.g. grey areas near $\lambda_i \cong 1595nm$, $\lambda_s \cong 1570nm$ and vice versa). However there are many (λ_i,λ_s) combinations with high detuning where the efficiencies are much lower and hence averaging over all these detuning values is a much more representative tunability measure. Once η_0, $\Delta\lambda$ and $\delta\lambda$ are obtained for a multitude of P_0 and L values we calculate EBT and EBT$_{PL}$ through maximization according to Eqs. (2) and (3). In this work we consider values of the incident pump power $0.1W \leq P_0 \leq 2W$ with 0.1W spacing and waveguide lengths $25\mu m \leq L \leq 500\mu m$ at $25\mu m$ spacing. Applying this procedure for the waveguide in question we find EBT=0.62nm^2 and EBT$_{PL}$=3.88fm/W for the waveguide in question in Figure 2.

Alternative waveguide designs can be obtained by repositioning the first and the second class of holes along the y-directions. Figure 3(a) and (b) plot the values of EBT and EBT$_{PL}$ with respect to Δy_1 and Δy_2 which are the perturbations of y_1 and y_2 shown in Figure 1. We sweep in a grid of $(\Delta y_1, \Delta y_2)$ values where $0.1a \leq \Delta y_1 \leq 0.15a$ and $0 \leq \Delta y_2 \leq 0.1a$ spaced by 0.005a and 0.01a respectively. The ranges for these design parameters are chosen to ensure monomode operation. In Figure 4, we explore alternative waveguide designs where we perturb (y_1,r_1), i.e. the y-positions and radii of the 1st class of holes. We use 0.004a spacing for the r_1 values. As illustrated in the figures, the largest EBT and EBT$_{PL}$ values are obtained in Figure 3(a) and 4(b) respectively. To better identify these designs we have performed the EBT and EBT$_{PL}$ calculations in a finer grid around the optimum parameters values of Figures 3 and 4. Table 1 summarizes the best designs for each case obtained in a tighter parameter range, $0.11a \leq \Delta y_1 \leq 0.14a$, $0.08a \leq \Delta y_2 \leq 0.1a$ and $0.23a \leq r_1 \leq 0.24a$. In the table, N_{avg} is the average free-carrier density obtained inside the flat band region.

Table 1. Waveguide designs

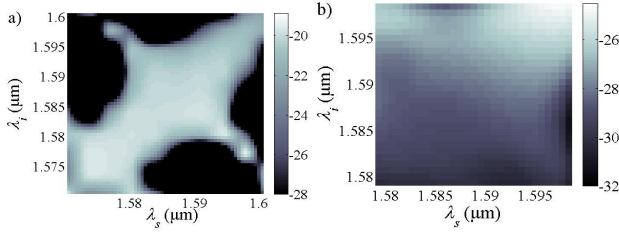| Parameter	Optimum with respect to EBT (Design A)	Optimum with respect to EBT$_{PL}$ (Design B)
EBT	1.96nm^2	0.2nm^2
EBT$_{PL}$	3.92fm/W	16.14fm/W
Δy_1	0.128a	0.124a
Δy_2	0.095a	unchanged
r_1	unchanged	0.235a
P_0	1W	0.1W
L	500μm	125μm
η_0	-18.3dB	-24.5dB
$\delta\lambda$	4.7nm	2.9nm
$\Delta\lambda$	28nm	19.6nm
N_{avg}	$5 \cdot 10^{18}$cm^{-3}	$18 \cdot 10^{18}$cm^{-3}

Figure 5. FWM conversion efficiency with respect to the signal and idler wavelengths for designs a) A and b) B, in Table 1.

To further validate the results we have computed η_0 values obtained for the designs A and B, using numerical solution of the ODEs for the values of P_0 and L quoted in the Table 1. Negligible differences are obtained for both designs. Figure 5(a) and (b) show the wavelength dependence of η for the designs shown in Table 1.

It is noteworthy that, as shown in Table 1 designing the waveguide by maximizing the EBT leads to relatively high efficiencies over a wide range of pump wavelengths and with significant tunability. However, this behavior is obtained at the cost of high pump powers and rather lengthy waveguides. This is not surprising since EBT does not explicitly take into account these two parameters. On the other hand, optimizing the design with respect to EBT$_{PL}$ results in lower efficiency values over somewhat narrower bandwidths $\Delta\lambda$ and tunability ranges $\delta\lambda$, but these waveguides are much shorter and require much less pump power. Moreover, according to [14] the power of the idler wave and as a consequence the FWM efficiency is experiencing a $(P_0L)^2$ dependence in the lossless case. Thus, it would be interesting to evaluate an alternative FoM similar to Eq. (3) but where a $(P_0L)^2$ term appears in the denominator instead of P_0L. Optimizing with this alternative FoM, results in almost the same design parameters as the design B of Table 1. However η_{max} for this design is significantly decreased due to $(P_0L)^2$ in the denominator which favors shorter waveguides with smaller efficiencies yielding $\eta_{max} \cong$-30dB for Δy_1=0.126a, r_1=0.236a, P_0=0.1W and L=50µm.

Table 2. FWM efficiency dependence on the loss mechanism.

Loss case	Design A		Design B	
	η_0	$P_p(L)/P_0$	η_0	$P_p(L)/P_0$
Only linear	-5dB	2.3dB	-20.5dB	0.69dB
Linear and TPA	-7.2dB	3dB	-20.9dB	0.8dB
Linear, TPA and FC	-19.2dB	9.5dB	-24.6dB	2.6dB

Another interesting aspect is the fact that FC effects seem to severely affect waveguide performance. To show this, we have numerically calculated the efficiencies and the pump loss for designs A and B under different loss conditions. Table 2, summarizes our findings for the cases where a) only linear losses, b) TPA and linear losses and c) all three loss mechanisms are assumed. The results indicate that including the TPA losses result in a small change in η_0 as well as the pump loss level. FC effects are more degrading: A significant efficiency drop of 12dB for design A and 3.7dB for design B is obtained when FC effects are accounted for. Since design B requires much less pump power and is shorter, the importance of nonlinear loss is less significant than the case of design A.

In conclusion we have discussed how PCW designs can be optimized by the proposed FoMs. Optimizing with respect to EBT tends to lead to large efficiencies with considerable bandwidths and wide tunabilities. Optimizing with respect to EBT$_{PL}$ yields shorter devices with smaller power requirements. One could also apply other similar FoMs depending on the application at hand and its requirements. We have also derived an approximate solution of the FWM efficiency which yields accurate results at only a fraction of the computational time compared to numerical solutions. Suitable PCW designs can be identified through exhaustive search and are characterized by relatively large FWM efficiencies over large bandwidths and wavelength detunings. The proposed design framework can play a useful role in designing PCWs, CROWs and highly nonlinear fibers for FWM-based signal-processing applications.

References

1. Y. Gong, J. Huang, K. Li, N. Copner, J. J. Martinez, L.Wang, T. Duan, W. Zhang, and W. H. Loh, *Opt. Express* **20**, 24030 (2012).
2. B. Corcoran, M. D. Pelusi, C. Monat, J. Li, L. O'Faolain, T. F. Krauss, and B. J. Eggleton, *Opt. Letters* **36**, 1728 (2011).
3. R. Salem, M. A. Foster, A. C. Turner, D. F. Geragthy, M. Lipson, and A. L.Gaeta, *Nat. Photonics* **2(1)**, 465 (2008).
4. F. Li, M. Pelusi, D-X. Xu, R. Ma, S. Janz, B.J. Eggleton, and D.J. Moss, *Opt. Express* **19**, 22410 (2011).
5. Q. Liu, S. Gao, L. Cao, and S. He, *JOSA B* **29**, 215 (2012).
6. J. Li, L. O'Faolain, and T. F. Krauss, *Opt. Express* **20**, 17474 (2012).
7. L. O'Faolain, S. A. Schulz, D. M. Beggs, T. P.White, M. Spasenović, L. Kuipers, F. Morichetti, A. Melloni, S. Mazoyer, J. P. Hugonin, P. Lalanne, and T. F. Krauss, *Opt. Express* **18**, 27627 (2010).
8. P. Kanakis, T. Kamalakis, and T. Sphicopoulos, *JOSA B* **29**, 2787 (2012).
9. T. Chen, J. Sun, and L. Li, *Opt Express* **20**, 20043 (2012).
10. C. Monat, M. Ebnali-Heidari, C. Grillet, B. Corcoran, B. J. Eggleton, T. P. White, L. O'Faolain, J. Li, and T. F. Krauss, *Opt. Express* **18**, 22915 (2010).
11. A. C. Turner-Foster, M. A. Foster, J. S. Levy, C. B. Poitras, R. Salem, A. L. Gaeta, *Opt. Express* **18**, 3582 (2010).
12. S. Rawal, R. K. Sinha, and R. M. De La Rue, *J. Nanophoton.* **6(1)**, 063504 (2012).
13. L. F. Shampine and M. K. Gordon, Computer Solution of Ordinary Differential Equations: the Initial Value Problem, W. H. Freeman 1975.
14. K. O. Hill, D. C. Johnson, B. S. Kawasaki, and R. I. MacDonald, *J. Appl. Phys.* **49**, 5098 (1978).